Spin noise fluctuations from paramagnetic molecular adsorbates on surfaces

Paolo Messina,[a] Matteo Mannini, Andrea Caneschi, Dante Gatteschi, and Lorenzo Sorace
Department of Chemistry and INSTM Research Unit, University of Florence, 50019 Sesto Fiorentino, Italy

Paolo Sigalotti, Cristian Sandrin, and Stefano Prato
APEResearch, Science Park Area, Campus Basovizza, 34012 Trieste, Italy

Paolo Pittana
Elettra Synchrotrone Laboratory, Science Park Area, Campus Basovizza, 34012 Trieste, Italy

Yishay Manassen
Department of Physics, Ben Gurion University of the Negev, P.O. Box 653, Beer Sheva 84105, Israel

(Received 2 May 2006; accepted 5 December 2006; published online 14 March 2007)

The measurement of spin noise in nuclei was demonstrated on bulk samples more than two decades ago. An ensemble of spins can produce a coherent signal at the Larmor frequency of a static magnetic field, known as spin noise, an effect due to the statistical polarization of small ensembles. The difficulty of these measurements is that the signal is extremely small—even if electron spins are detected. Although the statistical polarization of N spins dominates the Boltzmann statistics if N approaches unity, a more sensitive tool is requested to measure the polarization of the magnetic moment of a single spin. In this paper we report on the verification of recent results on the detection of spin noise from paramagnetic molecules of α,γ-bisdiphenylene-β-phenylallyl (BDPA) by Durkan and Welland [Appl. Phys. Lett. **80**, 458 (2002)]. We also present results on a second paramagnetic specie 1,1-diphenyl-2-picrylhydrazyl (DPPH), deposited on Au(111) surfaces. Electron spin resonance spectra from ultrathin films of DPPH and BDPA grown on Au(111) are reported. We prove that the paramagnetic molecules preserve their magnetism on the surface. These data and a thorough analysis of the signal recovery apparatus help us to understand the low statistical recurrence of the spin noise in the data set. A detailed description of the experimental apparatus together with an analysis of the parameters that determine the sensitivity are also presented. © *2007 American Institute of Physics*. [DOI: 10.1063/1.2434832]

I. INTRODUCTION

An ensemble of N spins of magnetic moment μ can produce a statistical polarization of its magnetization proportional to $N^{1/2}\mu$ without the application of any driving radio frequency (rf) field. These measurements have received much attention since the detection of spin noise from ^{35}Cl represent one of the fundamental issues in magnetic resonances.[1–3] In fact, the observation of magnetic resonance through the detection of the statistical polarization of the magnetic moments can open up the possibility to detect the spin dynamics of small ensembles.[3] In these systems a conventional probing apparatus might disruptively interact with the system under investigation. There is therefore a need for probes that do not alter the state of the physical system under investigation. In recent experiments[3] the detection of spin noise has led to determine g factor, electron spin, nuclear spin, hyperfine splitting, nuclear moment, and spin coherence lifetime of a small ensemble of electron spins.

Coherence effects may be observed even for a single spin system after averaging over a time period much longer than all relevant time constants in the system. This ergodic nature of the individual spin dynamics has allowed the detection of single spins by means of fluorescence experiments.[4]

Specifically our interest towards the detection of spin noise arises from the possibility of studying individual molecules of molecular nanomagnets. Molecular nanomagnetism is a rapidly developing research field[5,6] whose aim, among others, is the design of molecules with desired magnetic properties. In this framework clusters possessing giant spins as high as $S=83/2$ have been reported.[7] Detection of spin noise fluctuation is a promising technique to unveil the magnetic dynamics of these systems at the single molecule level. On the other hand, molecular nanomagnets might be particularly suited as benchmark tool for the development of techniques to probe single spin dynamics.

The possibility of the detection of a single spin magnetic moment from its statistical polarization by means of scanning tunneling microscopy (STM) has been successfully proven more than a decade ago by one of the authors.[8] In the reported experiment the authors located a STM tip over a defect in oxidized silicon surface with a static magnetic field applied perpendicular to the surface plane. This experiment was earlier defined as ESR-STM;[8] however what is actually detected by STM is the coherent Electron SPIN Noise in-

[a]Author to whom correspondence should be addressed; present address: Material Science Division, Argonne National Laboratory, 9700 S. Cass Avenue Argonne, IL 60439; electronic mail: pmessina@anl.gov

duced by the natural precession of the spin in a static magnetic field. We then believe that the acronym ESN-STM (Electron Spin Noise-STM) is better suited to describe this phenomenon.

Recent results[1,9] have proven that ESN-STM can be detected not only in dangling bonds at silicon surfaces but also looking at organic radicals deposited on highly oriented pyrolytic graphite (HOPG) surfaces. By locating the STM tip over an assembly of organic radicals the authors were able to detect a peak for a molecular system with electron spin $S=1/2$. The same authors have demonstrated that the technique is able to detect side peaks located at the position of the organic radical hyperfine levels.[9]

In this paper we present an experimental setup for single spin detection by ESN-STM, by verifying recent results on the detection of spin noise from paramagnetic molecules of α,γ-bisdiphenylene-β-phenylallyl[1] (BDPA) and focusing on a second paramagnetic species, 1,1-diphenyl-2-picrylhydrazyl (DPPH), deposited on Au(111) surfaces. The samples were preliminarily characterized by electron spin resonance (ESR) to obtain information about the magnetic properties of the molecules deposited on surface and the surface coverage.

It is worth stressing here that these two organic radicals are well known ESR standards and their properties in solutions have been thoroughly studied.[10,11] It is relevant to this study that for both species the electron spin is substantially delocalized on the entire molecule. This has implications on the electron spin dephasing process as explained in the discussion.

The difficulty of the experiment requires a thorough report on the technique and experimental apparatus we have built which will be given in Sec. II. Experimental details will be given in Sec. III while the obtained results will be discussed in Sec. IV. Further technical details on the apparatus are reported in the appendixes.

II. IMPLEMENTATION OF ESN-STM EXPERIMENT

A major experimental difficulty encountered in the realization of the ESN-STM experiments[1,12] lies in the fact that the signal level is quite low (it was estimated to be −120 dBm on a 50 Ω impedance line[1]) and inherently the signal to noise (S/N) ratio[1,9] amounts only to 4–5. It is not clear whether this low intensity is entirely due to the intrinsic physics of the observed phenomenon or whether it might be improved by a superior rf recovery circuitry.

The dependence of the mean square uncertainty in the measurement of the spectral density S, under certain approximations,[13] is inversely dependent on the observation time t:

$$\frac{\langle \Delta S \rangle}{S^2} = \frac{1}{(\mathrm{RBW})t}, \tag{1}$$

where RBW is the resolution bandwidth of the spectrum analyzer. The use of the STM to probe a spin center limits the observation time to a few seconds due to the thermal drift of the STM tip. On the other hand the field heterogeneity in the x, y, and z directions demands a frequency span of the measurements (typically from 10 to 20 MHz in our setup). These two experimental constraints are clearly in conflict with each other and create a major source of experimental difficulties in electron spin noise detected by STM. Furthermore unlike other experiments on spin noise fluctuations in spin ensemble[3,4,14] the dependence of the spectral density on the spin dynamics in STM experiments is largely unknown. A number of theoretical models have been recently reported but they have not been experimentally verified.[12,15–25] These theories postulate an interaction between the electron spins of the paramagnetic site and the tunneling electrons. Previous studies on spin noise[26] have outlined that a near field B_1 generated by the ensemble of spins itself is responsible for the induction of a voltage into pick-up coils. The importance of the near field in detecting single spins and small spin ensembles is also revealed by recent work in the field of spatially resolved spin detection.[27–29] Herein we do not refer to a specific model and associated spectral density to analyze our data.

We have used a general protocol presented by one of the authors to detect the low level rf signal from the STM tip.[13,30] A small oscillating magnetic field ΔB is added to the static magnetic field B_0. In this way the actual field at the sample is $B=B_0+\Delta B\cos(\omega_m t+\phi)$, where $\omega_m=2\pi\nu_m$ is the modulation frequency (ν_m in hertz) and ϕ is the phase. This is slightly different than the ac modulation introduced in an ordinary ESR experiment (see Appendix D). The resulting signal will occur at a frequency modulated in time $\omega=\omega_0+\Delta\omega\cos(\omega_m t+\phi)$, where ω_0 is the unmodulated frequency and $\Delta\omega=2\pi g\mu_B\Delta B/h$ is the frequency modulation intensity (here μ_B is the Bohr magneton, g is the Landé factor of the paramagnet, and h is Planck's constant). The Fourier transform of such a signal will result in a set of equally spaced sidebands with frequencies ω_0, $\omega_0\pm\omega_m,\ldots,\omega_0\pm n\omega_m$.[31] The intensity of the nth sideband will be given by an nth order Bessel function of the first kind, $J_n(m_\omega)$, where $m_\omega=\Delta\omega/\omega_m$ is the modulation index. The number of sidebands is roughly given by $2m_\omega$ so that the total width of the spectrum is given by $2\Delta\omega$. If the modulation index is chosen as $m_\omega=\Delta\omega/\omega_m=2$, the components of the Fourier spectrum J_1 will be maximized and inherently a phase sensitive detection (PSD) will provide the highest sensitivity in the detection of the signal.[13]

Figure 1 shows the setup we have used to detect spin noise fluctuation. The video output of the spectrum analyzer is fed into a lock-in amplifier referenced at $\omega_m=2\pi\nu_m$. The spectrum analyzer is actually a superheterodyne detector with three mixers that convert the input signal frequency to an intermediate frequency (i.f.) and then filters the high frequency components through a bandpass filter. The signal from the bandpass filter is detected by an envelope detector. The envelope detector provides a low frequency signal proportional to the absolute value of the i.f. signal $V_{\mathrm{out}}=\langle|V_{\mathrm{if}}|\rangle$. If the bandpass filter has a resolution bandwidth of the same order of the modulation frequency ($\mathrm{RBW}\approx\nu_m$) a PSD can be used. The line shape of the lock-in amplifier output will be dependent on a number of parameters and, in particular, on the ratio between the sweep time (SWT) and the lock-in time constant τ_{PSD}. When the latter is smaller than 1% of

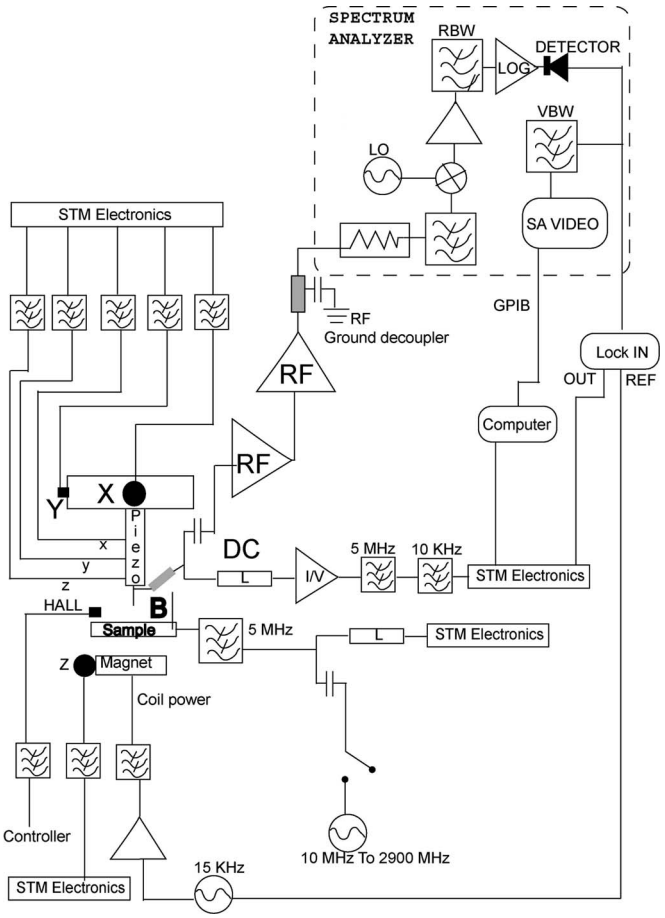

FIG. 1. Detection scheme for ESN STM. The signal is recovered from the STM tunneling current and is split into the dc and ac parts. The ac part is then amplified and detected by a spectrum analyzer (SA). The video output of the SA is connected to the input of a lock-in amplifier which detects the component of the signal in phase with the ac magnetic field. The part within the dashed line illustrates the function of the SA: the signal is sampled and mixed with a reference signal produced within the analyzer. The mixed signal is filtered and amplified. The width of the filter (RBW) sets the frequency resolution with which a spectral feature can be resolved. As explained in the text the RBW and the lock-in integration time determine the time of a single span. The picture shows also the extensive filtering to spurious noise that has been implemented on this setup.

SWT and the intrinsic linewidth of the signal is larger than RBW the output of the lock-in amplifier will provide a derivative line shape. In principle in this situation the linewidth of the signal measured by the lock-in amplifier corresponds to the intrinsic one and is correlated with the spin longitudinal decay time T_1 and the phase memory time T_2.[3]

However, alongside with previous literature on single spin detection,[4] our results (see *infra*) demonstrate that the assumption that ω_0 is a constant over the time of measurement T_m is incorrect if the interaction of the electron spin with the surrounding is considered.

A more realistic picture is described by the following equation:

$$\omega(\tau) = \omega_0(t,T_1) + \Delta\omega \cos[\omega_m t + \phi(t,T_2)], \tag{2}$$

where $\omega_0(t,T_1)$ and $\phi(t,T_2)$ are random functions of the time with characteristic correlation times that are not known. In particular, $\omega_0(t,T_1)$ is a function containing the dependence of the central frequency on the hyperfine interaction and on

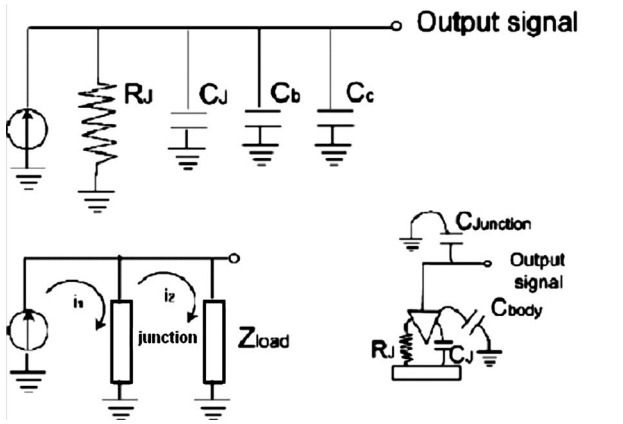

FIG. 2. The tunnel junction and the cable connections to the rf preamplifier are schematically shown as a current generator with a parallel impedance. The impedance has a resistive part and several capacitances. The origin of the several capacitances is illustrated in the drawing on the bottom right. The junction capacitance C_j accounts for both the geometrical capacitance and the quantum capacitance (see text and references). In order to transfer the maximum signal to the rf amplifier (Z_{Load} in the drawing on the bottom left) the sum of the capacitances must be minimized. This is achieved by shortening the distance between the STM tip and the rf preamplifier.

the g anisotropy; it depends on the longitudinal relaxation time T_1; $\phi(t,T_2)$ is the function containing the dependence of the phase on the transverse relaxation time, T_2.

While single spin detection by magnetic resonance force microscopy (MRFM) is sensitive to the spin flip in the z component of the spin vector,[28] our setup is sensitive to the x and y components of the spin vector precessing around the z axis. As a result T_1 will mostly determine the time scale of frequency jumps, whereas T_2 will determine the time scale of the fastest spin sensitive interaction between the paramagnetic molecule and the probe. For ESN-STM there is no simple way to correlate the measured parameters to the intrinsic spin dynamics time constants, T_1 and T_2.

Another important aspect of our detection apparatus is the amplification and the overall noise figure. We have designed and constructed a rf recovery circuitry that can detect a low level signal in a relatively wide band (50–1500 MHz). There are two important duties that the recovery circuitry should accomplish: recover the maximum signal power available and amplify the signal without a severe degradation of the S/N ratio.

In order to achieve the former, the best solution is to place the first amplification stage as close as possible to the signal source, i.e. to the tunneling junction. Indeed, part of the signal can be lost into connections with the ground provided by several parasitic capacitances and this loss should be minimized. Figure 2 illustrates a schematic of the tunneling junction with its parasitic capacitances where C_T is the tunnel junction capacitance, C_c the connection capacitance (due to the connection between the source and the first amplification stage), and C_B is the STM tip-body capacitance. In this paper we consider the junction capacitance C_T to be purely geometrical. The cable connecting the STM tip to the rf preamplifier has been chosen to minimize C_c. A perfect impedance matching between the cable and the STM tip termination over the entire frequency range of interest would not be possible. Since the rf preamplifier is located close to

the STM tip, the amount of signal backscattered at the cable-tip junction will be minimized for signal frequencies corresponding to a wavelength bigger than the STM tip length. This is indeed the case for ESN-STM.

The sensitivity, i. e. the minimum signal power that a receiver can detect, depends on the temperature, the band width in which the signal is detected and on the degradation of the signal to noise ratio introduced by the receiver itself. The sensitivity, S, is expressed in decibels and is defined as the signal power that would give a signal to noise ratio equal to 1:[32]

$$S = -174 + 10\log(\mathrm{RBW}) + \mathrm{NF}_{\mathrm{system}}, \tag{3}$$

where RBW is the spectrum analyzer resolution bandwidth and $\mathrm{NF}_{\mathrm{system}}$ is the noise figure of the entire recovery circuit. The value of −174 dBm is the noise produced by a resistive source at room temperature in the bandwidth of 1 Hz. The noise figure is a measure of the degradation of the signal to noise ratio introduced by the detector. In the case that the sum of the preamplification total gain and its noise figure is larger than 39 dB, the $\mathrm{NF}_{\mathrm{system}}$ value is expressed by the following formula:[32]

$$\mathrm{NF}_{\mathrm{system}} = G_{\mathrm{PA}} - 2.5\ \mathrm{dB}, \tag{4}$$

where G_{PA} is the gain in decibels of the preamplification stage and 2.5 dB is specific to log power averaging. The sensitivity, as already mentioned, is limited by the acquisition time. In nondigital filtering spectrum analyzer the acquisition time SWT critically depends on the RBW and the on the frequency range (SPAN) in which the spectrum analyzer searches for a signal:

$$\mathrm{SWT} = \frac{k \times \mathrm{SPAN}}{\mathrm{RBW}^2}, \tag{5}$$

where k is a constant.[32]

In cases in which the signal is very close to the noise level, video filtering is used to flatten the spectrum and make the signal more evident. In these cases the SWT depends also on the video bandwidth (VBW) filter as follows:

$$\mathrm{SWT} = \frac{k \times \mathrm{SPAN}}{\mathrm{RBW} \times \mathrm{VBW}}. \tag{6}$$

The minimum acceptable value for SPAN is given by the interval in which the signal frequency fluctuates for a given hyperfine level.[1,31] However, the widest span in which the signal must be recovered is given by the magnetic field measurement precision. Our spectrum analyzer is able to perform a span of 20 MHz (corresponding for an electron spin to about 7 G error bar in the measurement of the magnetic field) in 500 ms with RBW=10 kHz. We have taken RBW =VBW=10 kHz as design parameter for the rf recovery circuit. Also we have constructed a homebuilt rf preamplifier with a NF=1 dB in a frequency span of 50–1500 MHz. The I/V converter is incorporated in the same case as the rf preamplifier.

The frequency response of the rf amplifier is flat within 1 dB and the gain G is larger than 20 dB in the frequency range of interest. Further details are reported in Table I. In cascade to this amplifier we have connected a Minicircuits ZKL-1R5 amplifier capable of 40 dB gain over a bandwidth of 1500 MHz. The total gain of the preamplification stage ranges from 55 to 60 dB. The noise figure $\mathrm{NF}_{\mathrm{PA}}$ is 4 dB. The sum of these two values is larger than 39 dB, therefore Eq. (2) holds.[32] The $\mathrm{NF}_{\mathrm{system}}$ is then 1.5 dB. This means that the theoretical sensitivity of the recovery system for a SPAN value of 20 MHz and a RBW=10 kHz varies between −127.5 and −132.5 dBm as computed from Eq. (1).

TABLE I. Major features of the homebuilt low-level, low-noise rf amplifier. This amplifier is the first stage of the recovery circuitry.

Property	Value
Maximum gain	22.6 dB at 200 MHz
Bandwidth with gain ≥ 10 dB	32.6–4100 MHz
Bandwidth with gain ≥ 15 dB	45.5–2700 MHz
Bandwidth with gain ≥ 20 dB	73.8–1200 MHz
Minimum signal detected	−140 dBm at 500 MHz
Noise level reported to the input	−145 dBm at 500 MHz
Input impedance	50 Ω
Out impedance	50 Ω
Power supply	20–30 V
Current demand	<30 mA

Filtering of the rf environmental noise has proven to be crucial to the success of the experiment reported below. For this reason all the cable connections to the vacuum chamber have been filtered. Piezodrivers, motors, and Hall probe connections have been filtered at the feedthroughs of the vacuum chamber by means of homebuilt passive rf filters. These filters feature 70 dB of attenuation above 10 MHz. rf spurious noise is filtered also at the tunneling current and bias voltage connections. rf harmonics due to digital equipment have been eliminated.

The connection between the second rf amplifier and the spectrum analyzer has been decoupled from the ground with a homebuilt SMA ground decoupler. It is a passive element with an attenuation larger than 2 dB below 2 GHz. This was necessary to reduce some low frequency noise that entered the STM through the spectrum analyzer.

We have tested the sensitivity of our experimental setup by simulating a real experiment: a rf signal is input into the tunnel junction; the entire experimental apparatus is set as in a real experiment with all the electronics equipment on (including field modulation); both unmodulated and modulated signals were input to compare spectrum analyzer detection only and spectrum analyzer detection combined with PSD.[3]

Table II reports the value of the sensitivity measured in the two cases at different frequencies. The PSD is more sensitive than spectrum analyzer stand alone detection. Also the derivative line shape of PSD recorded spectra is more evident to the experimentalist while looking for a low level signal than the sharp shape peak close to the noise level provided by spectrum analyzer detection.

Another aspect which was crucial for the success of our ESN-STM experiments was the implementation of a software that can handle in real time both STM operations and ESN-STM. A key point of this software is its ability to scan acquiring a STM image, stop scanning at the operator com-

TABLE II. Comparison between the sensitivities of the recovery circuit when a spectrum analyzer is used as a final detector and when a lock-in amplifier is used.

Frequency (MHz)	SA Sensitivity (dBm) SWT=4 s SPAN=6 MHz	SA sensitivity (dBm) SWT=4 s SPAN=3 MHz	Lock-in sensitivity (dBm) SWT=4 s SPAN=6 MHz	Lock-in sensitivity (dBm) SWT=4 s SPAN=3 MHz
100	−95	−93	−99	−98
200	−109	−109	−116	−117
300	−131	−130	−136	−139
400	−119	−119	−122	−122
500	−130	−130	−136	−136
600	−137	−137	−145	−147
700	−128	−125	−138	−135
800	−114	−116	−135	−137
900	−134	−133	−140	−137
1000	−138	−139	−144	−148

mand, position the tip over a target, modify tunneling current and bias voltage, trigger on the spectrum analyzer, acquire an ESN-STM spectra from the lock-in amplifier, and restart scanning, reiterating this cycle every time the operator decides. In this way the software allows for acquiring many spectra and the STM topography associated with it and makes statistical analysis of the results possible.

III. EXPERIMENTAL DETAILS

Samples for ESN-STM were prepared by immersing a flame annealed Au(111) 150 nm thick film evaporated on mica into CH_2Cl_2 solutions of DPPH and BDPA, respectively (purchased from Sigma Aldrich, Inc.). The solution concentration has been varied from 0.1 to 0.01 mM and the exposure time from 1 to 15 min in order to evaluate different degrees of coverage and to optimize the deposition quality. The sample was then rinsed three to four times for 10–30 s into pure CH_2Cl_2 and dried under nitrogen fluxing.

STM imaging and ESN-STM were performed under ambient conditions. The vacuum chamber is sealed and is used to insulate the experimental setup from environmental rf spurious noise. The ESN-STM measurements reported in the following have been achieved under the application of an ac and a dc magnetic field. The ac field magnitude was 10 mG corresponding to a modulation index $m_\omega=2$ for a modulation frequency $\upsilon_m=15$ kHz. The ac field was measured using the Sypris gaussmeter applying a field of 0.1–0.5 G and extrapolating the value of the voltage amplitude to achieve a field of 10 mG. Once the sample was mounted on the sample holder all components (namely, x, y, and z) of the dc magnetic field on the sample were measured carefully with the same gaussmeter.[33] The precision varied between 2 and 4 G depending on the size of the sample mounted on the sample holder.

In order to distinguish between ESN-STM spectra and the environmental noise at the same frequency, over 600 spectra were taken with the tip slightly retracted and out of tunneling. The entire experimental apparatus was set up as for measurements performed with the tip in tunneling. Indeed peaks in the spectral density of the tunneling current can arise from voltage fluctuations at the rf amplifier input and/or at the modulating coils. This circumstance needs to be ruled out.[26] After acquiring the spectrum from the lock-in amplifier in these conditions, the three most intense peaks per spectrum were analyzed. The peak to peak amplitude P_{kk}, divided by the standard deviation σ, is the parameter that was used as statistical indicator.

Continuous wave ESR (cw-ESR) spectra were acquired using a Bruker Elexsys E500 spectrometer working at the X band ($\nu\sim9.4$ GHz) equipped with a Super-High-Q (SHQ) cavity. Ultrathin film samples for investigation with this technique were obtained by incubating Au(111) flame annealed slides for 4 h in CH_2Cl_2 0.1 mM solutions of the radicals.

IV. RESULTS AND DISCUSSION

A. STM

Figures 3(a) and 3(b) show typical images observed for DPPH and BDPA molecules deposited on Au(111) surfaces. As the geometrical size of the smallest white spots corresponds to DPPH and BDPA molecular size within experimental error, we attribute them to DPPH and BDPA single molecules. Larger white spots indicate the formation of agglomerates of two or few molecules. ESN-STM signal reported herein was always obtained from single molecules.

Molecules deposited by spontaneous adsorption from diluted solutions did not form agglomerates with a large vertical size as found in samples prepared by drop casting.[1,9] STM imaging was achieved only for tunnel currents below 30 pA. The obtained STM images of the molecules are elongated along the scanning direction. We attribute this effect to an internal reorientation of the molecule caused by the tunneling current. Similar effects were reported recently.[34]

A relevant issue is whether the difficulty of STM imaging is related to molecular diffusion processes on Au(111). The diffusion properties of DPPH and BDPA on Au(111) are not known. However, several studies have been conducted by ultrahigh vacuum variable temperature STM to determine migration energy and diffusion constants of large adsorbates on metal surfaces.[35] The hopping rate of the molecule on the surface depends on the molecular surface interaction, the sur-

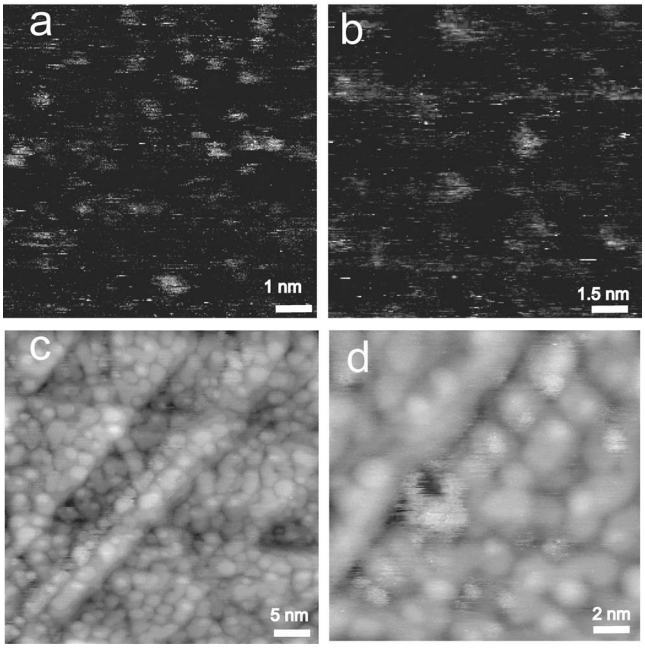

FIG. 3. (a) STM image (10×10 nm^2) of DPPH molecules deposited on Au(111). Tunneling current I_t=10 pA, bias voltage (BV)=0.1 V. (b) STM image (15×15 nm^2) of BDPA molecules deposited on Au(111). I_t=50 pA, BV=0.1 V. (c) STM image (50×50 nm^2) of BDPA small agglomerates on Au(111) formed 36 h after soaking. I_t=50 pA, BV=0.1 V. (d) STM image (20×20 nm^2) of BDPA small agglomerates on Au(111) formed 36 h after soaking. I_t=50 pA, BV=0.1 V.

face geometry, and also the surface coverage with molecular adsorbates. Both DPPH and BDPA are molecules containing several aromatic rings that can interact with noble metals via π interaction. In the case of molecules like C_{60} the migration energy on Au(111) is 1500 meV[35] and as a result diffusion is basically precluded at room temperature. Other molecules like PVBA [4-*trans*-2-(pyrid-4-yl-vinyl) benzoic acid, a molecule with two phenyl rings] deposited on Pd(110) have a hopping rate of about 0.01 Hz at room temperature.[35] On the basis of the data collected on other molecules we can then conclude that on average the molecule under the STM tip will not diffuse away during spectroscopy at the coverage we used. STM images acquired after a spectrum was taken on a molecule demonstrate that this did not change its position.

Figures 3(c) and 3(d) show ordered agglomerates of BDPA molecules. These are formed after 24–36 h from deposition. Once the molecules are laterally confined on the surface the STM image quality improves as long as the tunnel current is confined below 50 pA. These observations are similar to those reported by one of the authors on molecular complexes, which lead to ruling out long range diffusion as a result of the lateral confinement of neighboring molecules.[36]

B. Continuous wave ESR

cw-ESR measurements on ultrathin films of BDPA and DPPH radicals were used as a preliminary characterization tool to get information about the amount of deposited radicals, the level of aggregation of the samples, and the effect of deposition procedure on the magnetic properties of the deposited material. A single ESR signal is observed at g=2.005(5) for BDPA and at g=2.003(6) for DPPH, with no evidences for hyperfine structure (see Fig. 4). While this is in contrast with a solution spectrum for DPPH, for which the expected five line pattern[37] due to the hyperfine coupling with two almost equivalent ^{14}N I=1 nuclei is observed (coupling with ^{1}H being unresolved), a solution spectrum of BDPA in CH_2Cl_2 shows a single line with 7 G linewidth, as reported in literature.[38]

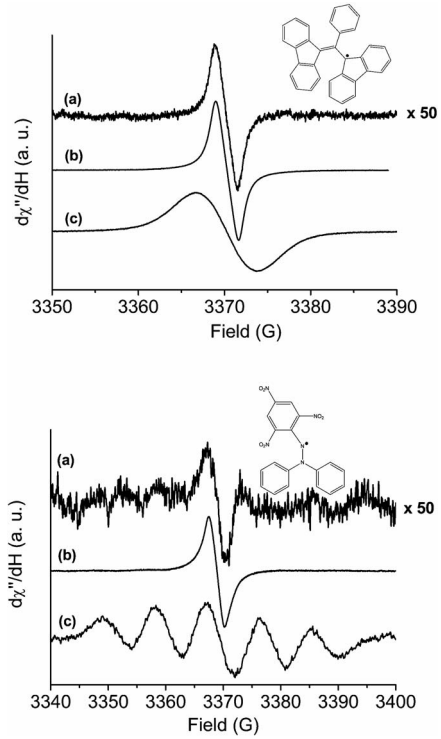

FIG. 4. Upper: Room temperature cw-ESR spectra of BDPA (molecule sketched in the upper right inset) as ultrathin film sample (a), drop cast sample from a solution 100 μM (b), and dichloromethane 10 μM solution (c). Lower: Room temperature cw-ESR spectra of DPPH (molecule sketched in the upper right inset) as ultrathin film sample (a), drop cast sample from a solution 100 μM (b), and dichloromethane 10 μM solution (c). For both molecules the intensity of ESR spectrum of ultrathin film is multiplied by a factor of 50 to be compared with that of drop cast sample, acquired in the same conditions.

Accurate information about the degree of molecular aggregation could in principle be provided by a comparison of spectral line shape and/or linewidths with solution and solid state spectra. Unfortunately, due to the low intensity of the signal we had to overmodulate (modulation amplitude of 3 G) the spectra to obtain a reasonable signal to noise ratio. This, coupled with the relatively large base line correction, induces a sizable line shape distortion and makes a detailed analysis impossible. It is, however, interesting to note that for both radicals the observed peak to peak linewidths, even if overmodulated, are smaller than those observed for dilute solutions with low modulation (0.3 G) while being broader than the corresponding solid state spectra. If one also considers the absence of hyperfine structure, it can be concluded that the spectra are dominated by the contribution of small molecular aggregates for which exchange narrowing processes are active.[39–41]

In this respect a comparison of the doubly integrated signal with standards containing known amount of spins sug-

gests that within the inherent limitations of quantitative ESR spectroscopy[42] the number of spins on each gold slide is of the order of 10^{12}. If one considers an optimal packing (i.e., a surface occupation for each molecule of BDPA and DPPH of 130 and 140 $Å^2$, respectively) this yields for both molecules a surface coverage of about (15±3)%. The relatively low coverage suggests that the presence of a sizable amount of isolated molecules, which by STM images have been shown to coexist on surfaces with molecular aggregates, can be considered as probable. We stress here that the spectrum of ultrathin films is far less intense than that obtained by drop casting method (see Fig. 4) with an approximate ratio of 1:50. This implies that for the latter method used, e.g., by Durkan and Welland for preparing ESN-STM samples,[1] the formation of multilayer and aggregates is much more probable.

A final observation concerns the effect of incubation time over the number of spins, as determined via ESR, deposited on gold. For DPPH it is clearly seen that this number increases with increasing time deposition (30 min–4 h). It is probable that this will result in an easier formation of aggregates for longer time of exposure. This is an important point to be considered, as samples for ESN-STM were incubated for a much shorter time than those for cw-ESR; it is then conceivable to assume that the number of molecular aggregates will be reduced in those samples.

In conclusion, cw-ESR spectra were used to prove that the paramagnetic character of a large number of BDPA and DPPH molecules is retained after deposition on gold. Further they suggest that the obtained coverage is limited to about 15%. As a consequence, the presence of large aggregates is less probable in samples prepared with the deposition method described here than in those obtained by drop casting,[1] thus making the former better candidates for observation of ESN-STM on single molecules.

C. ESN-STM

The statistical distribution of over 1800 noise fluctuations extracted from spectra obtained with the tip slightly retracted and out of tunneling is shown in Fig. 5. The analysis of the peak evidences that the value P_{kk}/σ for these spurious signals due to environmental noise was never larger than 6.7. Similar measurements carried out with the tip in tunneling regime over a bare Au(1,1,1) surface proved that also in this case the value P_{kk}/σ is always smaller than 6.7.

In the following we report only on the ESN-STM peaks with a value of $P_{kk}/\sigma \geqslant 7$. The statistical distribution reported in the inset of Fig. 5 shows the distribution of P_{kk}/σ for successful ESN-STM measurements.

Over 3300 ESN-STM spectra were measured on samples as described above. Only 0.5% of them resulted in ESN-STM spectra. Figure 6(a) shows the ESN-STM peak at 650.5 MHz (232.3 G) measured on the DPPH molecule evidenced by a circle in Fig. 6(b). The peak has a derivative shape as reported in previous work.[13] In this specific case the tunnel current during spectroscopy was raised to 0.6 nA while scanning was achieved at 30 pA. When a peak appeared in the spectrum the position of the tip was always

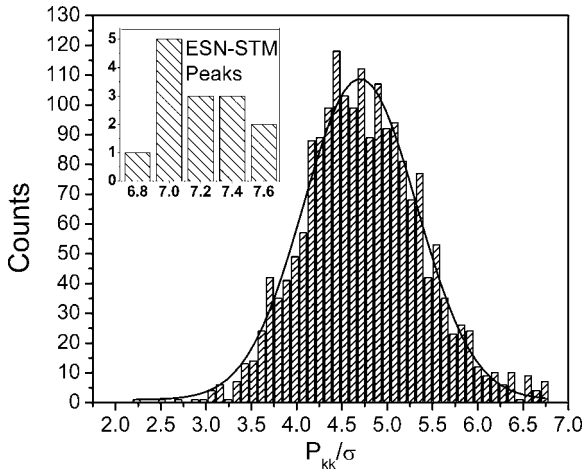

FIG. 5. Distribution of the amplitudes of the three largest noise fluctuations in over 630 spectra taken with the tip slightly retracted and out of tunneling. The value of the peak is normalized with respect to the standard deviation of each spectrum acquired. Inset: Distribution of ESN-STM peaks showing a value $P_{kk}/\sigma \geqslant 7$.

localized on a single molecule. As only 0.5% of the spectra taken resulted in ESN-STM spectra, we cannot rule out the possibility that the observed ESN-STM signal from a single molecule might also be somehow affected by the nearby presence of an agglomerate of two to three molecules.

Figure 7(a) reports the dependence of the peak position in the ESN-STM spectrum at different values of the applied dc magnetic field. The theoretical linear dependence of the Larmor frequency with varying magnetic field, which is the most important indicator for spin detection,[28] is verified.

Figures 7(b)–7(d) illustrate the shape and the magnitude of the peaks at 651.7, 539.1, and 427.3 MHz, corresponding to fields of 232.75, 192.5, and 152.6 G, respectively. At each field the experiments were done in a range of frequencies of about 20 MHz [the vertical bars in Figs. 6(a) and 7(d), one single scan was never larger than 10 MHz]. Nevertheless the signals were observed at the right frequency with a precision of 3 MHz. This shows that signals are not observed at frequencies different from the Larmor frequency.

Finally we have reproduced Durkan and Welland's results on BDPA. The tunneling current during ESN-STM spectroscopy is always confined in the range of 0.3–0.6 nA, less than half the value reported in Durkan and Welland's experiments.[1,9]

Figure 8(b) reports the ESN-STM spectrum detected on the BDPA molecule highlighted in Fig. 8(a). This spectrum was measured with a lock-in amplifier sensitivity of 200 μV and has to be compared with the spectrum in Fig. 9(c) where the same lock-in sensitivity for measurements on DPPH has been used. The frequency at which peaks occur is consistent with the measured magnetic field, as illustrated in Fig. 8(d). The uncertainty in this case is higher than that reported in Fig. 7(a) as only the sample position on the plane is varied, while the magnet z position is always constant (effect of B inhomogeneity in the x and y directions).

An analysis of the bandwidth of the signal observed for DPPH reveals a nonmonotonic dependence of the bandwidth on the frequency. Peaks found at the lowest frequency

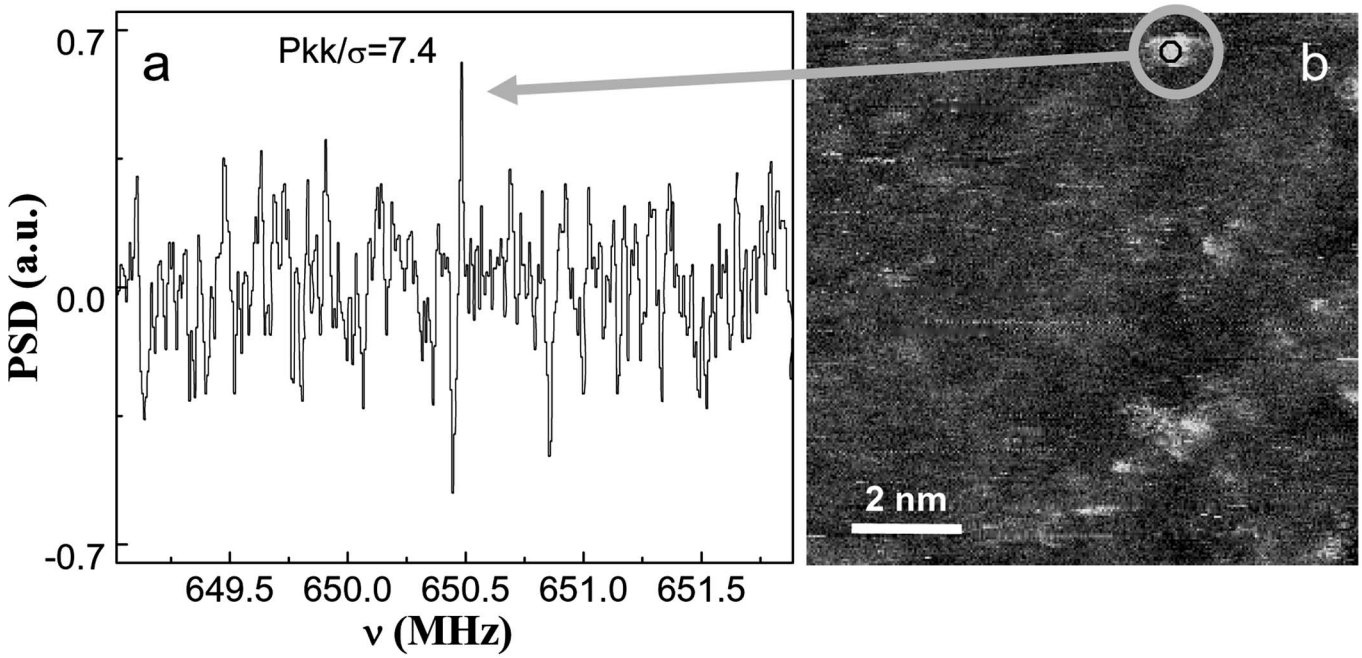

FIG. 6. (a) ESN-STM spectrum of DPPH deposited on Au(111) showing a peak at 651.5 MHz (232.7 G). SPAN=649–652 MHz, BW=VBW=30 kHz, SWT=6 s. The parameters during ESN-STM measurement were tunneling current 0.6 nA and bias voltage 0.3 V. ac field modulation frequency and intensity: 15 kHz, 10 mG. Lock-in sensitivity 1 mV, time constant 10 ms. (b) STM image (10×10 nm^2) of the molecule in (a). Experimental conditions during STM imaging: I_t=30 pA, BV=0.3.

(150 G region) have a width larger than 400 kHz whereas peaks at 540 and 650 MHz (190 and 234 G) regions have bandwidths that span from 100 to 300 kHz. Comparison between DPPH and BDPA peak widths for fields in the 234 G region shows values that are comprised in the range of 100–300 kHz.

V. DISCUSSION

The intensity of the ESN-STM peaks measured for both DPPH and BDPA can be estimated by adding the value of the signal to noise ratio measured in decibels to the sensitivity calculated according to Eq. (3). If we assume that the bandwidth of the narrower filter in the detection chain is proportional to the inverse of the lock-in time constant (10 ms), the intensity of the ESN-STM signal varies between −129 and −130.5 dBm (S/N ratio is comprised between 3 and 1.65 dB). This value is lower than that reported by Durkan and Welland[1] for BDPA even if it has to be noted that for those experiments no statistical data on success rate and amplitude distribution were reported. The magnitude of the PSD peak detected by one of the authors was also higher.[13,30] We believe that this is the result of a complex relationship between the spin dynamics of individual paramagnetic centers, their electronic structure, and our detection apparatus. We will analyze this problem in detail in the following.

The ruling concept herein is that the spectrum analyzer relies on a bandwidth filter that is swept across a certain span of frequencies. A signal can be reliably detected only if it is present at a given frequency for the entire duration of the sweep. If the signal has a transient nature with an intrinsic instability in frequency, the spectrum analyzer might fail to detect it. In the following we discuss a number of causes that might make the signal transient and therefore decrease the probability that it can be captured at the right time. This is particularly true if the sweep rate is slowed down and the time scale of the transient signal duration is small compared to this rate.[43]

In our experimental setup the sweep speed has been decreased to enable the use of a lock-in amplifier and our ESN-STM spectra are acquired for a time of up to 6 s. This is a time scale in which the molecule can undergo conformational modifications several times.[34] As a result the molecule might be in a state that does not produce a spin signal at the moment in which the bandwidth filter is tuned at the Larmor frequency.

Moreover the hyperfine interactions in BDPA and DPPH reduce the amplitude of the detectable signal by spreading the actual band in which the signal can be found over a range of about 50 MHz.[10,11] When the STM tip is brought over a molecule to detect the signal the receiver is tuned to the Larmor frequency of the central m_I level within a band of 10 MHz. There is, however, a possibility that during the measurement the level populated is a different m_I one. If the time of observation is long enough and the bandwidth of the receiver covers the entire hyperfine frequency range $\Delta\omega_I$, then the ESR spectrum of a single spin can be extracted.[4] In other words, hyperfine interactions can lead to an ESN-STM transient signal depending on the nuclear spin flip rate. The nuclear spin flip rate can be enhanced by the presence of a nearby unpaired electron spin. This phenomenon has been known for nuclei close to paramagnetic impurities in crystals[44] and depends on the electron spin longitudinal decay time T_1. Because the unpaired electron in both DPPH and BDPA is delocalized over the entire molecule[10,11] several nuclear spins (the most relevant ones are the ^{1}H atoms with

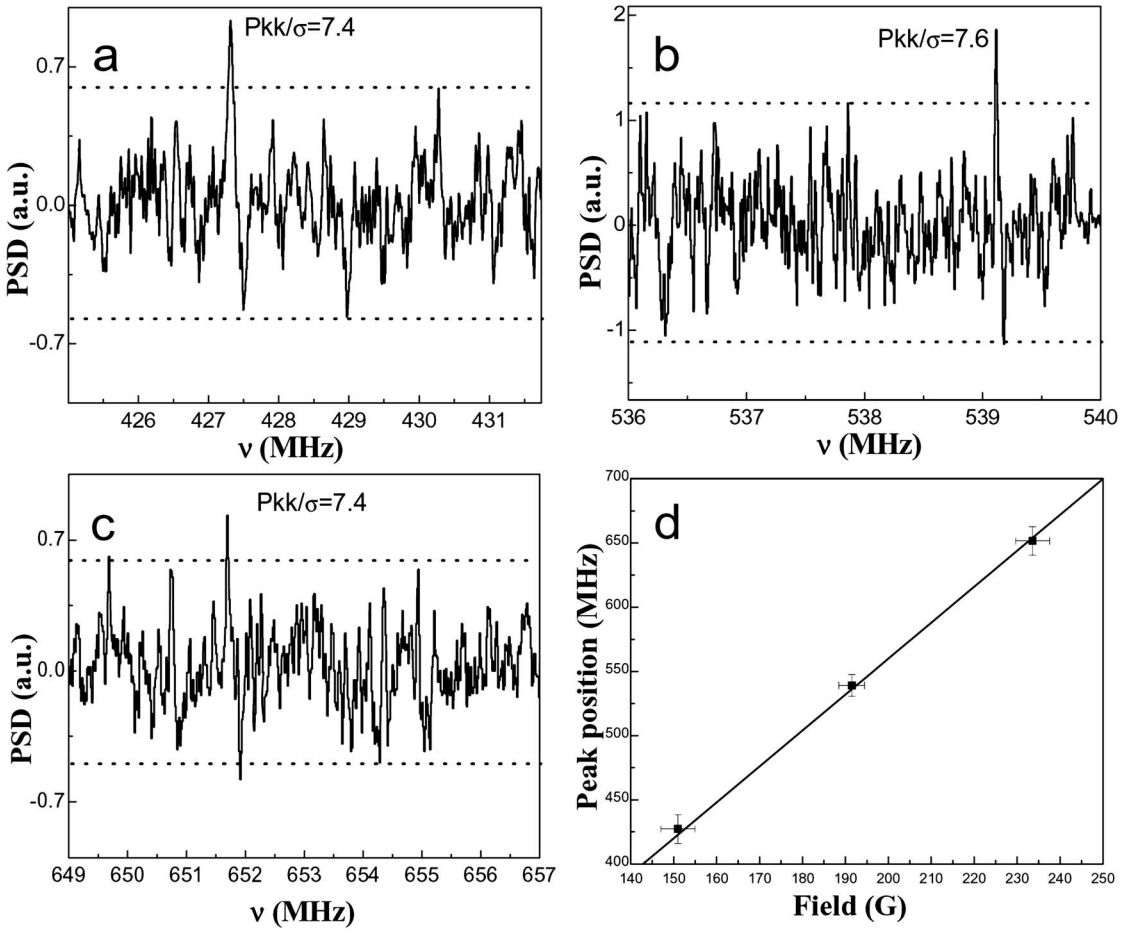

FIG. 7. (a) ESN-STM spectrum showing a peak at 427.13 MHz (152.54 G). SPAN=425–432 MHz, BW=VBW=30 kHz. SWT=6 s. Tunneling current during spectroscopy 0.3 nA. Bias voltage during spectroscopy 0.3 V. AC field modulation 15 kHz, 10 mG. Lock-in sensitivity 1 mV, time constant 10 ms. (b) ESN-STM spectrum showing a peak at 539.1 MHz (192.5 G). SPAN=536–540 MHz, BW=VBW=30 kHz. SWT=6 s. Tunneling current during spectroscopy 0.3 nA. Bias voltage during spectroscopy 0.3 V. AC field modulation 15 kHz, 10 mG. Lock-in sensitivity 1 mV, time constant 10 ms. (c) ESN-STM spectrum showing a peak at 651.68 MHz (232.7 G). SPAN=648–658 MHz, BW=VBW=30 kHz, SWT=6 s. Tunneling current during spectroscopy 0.6 nA. Bias voltage during spectroscopy 0.3 V. AC field modulation 15 kHz, 10 mG. Lock-in sensitivity 1 mV, time constant 10 ms. (d) Position of ESN-STM peak measured at different values of the DC magnetic field applied. The horizontal error bars represent the precision in the magnetic field measurement. The vertical bar indicates the frequency range in which the ESN-STM signal was searched. The line is calculated from the formula $\nu=(1/2)g\mu_B B$, in units of MHz and Gauss: $\nu(\mathrm{MHz})=2.8(\mathrm{MHz/G})\times B(\mathrm{G})$.

$I=1/2$ and, only for DPPH, the ^{14}N atoms with $I=1$) might flip during the measurement, leading to a possible change in the energy of the electron spin state occupied. A direct measurement of the nuclear ^{14}N and ^{1}H longitudinal relaxation time has not been reported in literature. However, a recent study of samples of BDPA dispersed in polystyrene shows that the electron spin relaxation time T_1 for the BDPA at room temperature is 42 μs.[45] In general crystalline organic radicals or concentrate solutions show $T_1=T_2$ due to exchange narrowing; however, in a more dilute environment T_1 becomes longer than T_2 and dependent on the temperature.[46] Early studies[47–49] of BDPA in solutions (10^{-2} mol/dm^3) report a T_1 of the order of 1 μs while other studies[11] report 0.5 μs. The value of T_1 for DPPH appears to be slightly slower but on the same order of magnitude.[50,51] We can therefore assume that the actual T_1 for the molecules of BDPA and DPPH deposited on Au(111) will be a value in the range of 1–42 μs. This situation does not apply to the Pb centers that were previously investigated by ESN-STM from one of the authors.[31] Indeed T_1 for paramagnetic impurities in a semiconductor is much longer than for BDPA and DPPH. This implies that the actual enhancement of the nuclear lon-gitudinal spin flip rate would be much reduced in a semiconductor as compared with our samples. Moreover, the natural abundance of ^{29}Si ($I=1/2$) is low (4%) and most of the Pb centers on SiO_2 surface do not present hyperfine coupling.[52–54]

The frequency at which the signal can be detected might also be affected by local electric field oscillations. However, this is true for Pb centers on SiO_2 rather than in organic radicals as reported in literature.[55] For organic radicals the effect of g anisotropy will produce a fluctuation of the spin noise frequency within a band of a 1–2 MHz. This can be calculated by taking into account some early publications on solid DPPH.[56,57] While these fluctuations fall in the bandwidth of our receiver they are larger than the signal width and are driven by the intramolecular motion which might be triggered by the tunneling current.[34] The g anisotropy is also present on Pb centers studied before but the alignment of the spin center with the direction of the magnetic field in a rigid lattice cannot change.

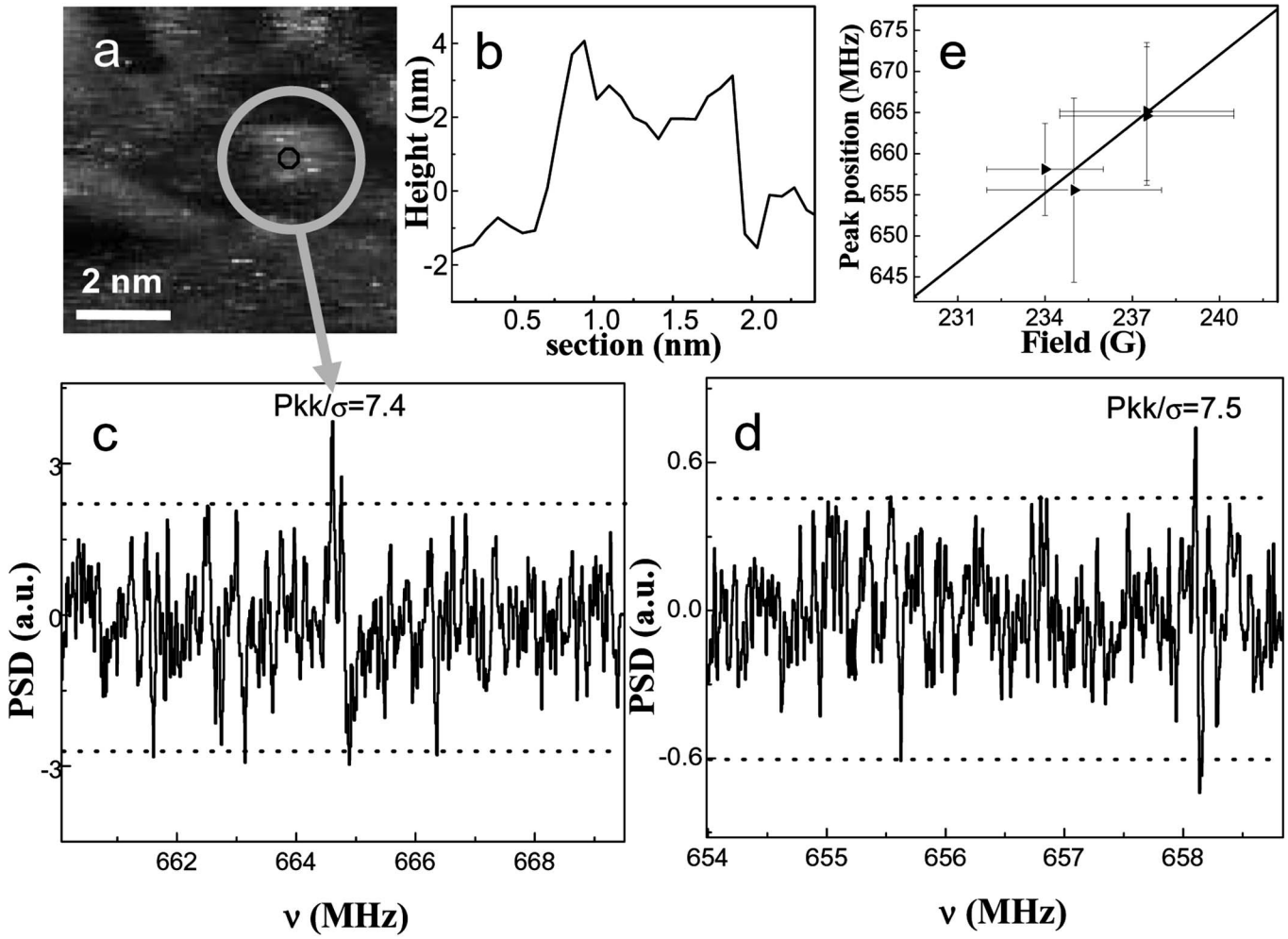

FIG. 8. (a) STM image (7×7 nm^2) of a BDPA molecule on which the ESN-STM spectrum reported in (c) is measured. I_t=30 pA, BV=0.3 V during STM imaging. (b) Profile of the BDPA molecule evidenced in (a). (c) ESN-STM spectrum showing a peak at 664.8 MHz (237.4 G). SPAN=660–670 MHz, BW=VBW=30 kHz. SWT=6 s. Tunneling current during spectroscopy 0.3 nA. Bias voltage during spectroscopy 0.3 V. AC field modulation 15 kHz, 10 mG. Lock-in sensitivity 200 μV, time constant 10 ms. (d) ESN-STM spectrum taken on a different BDPA molecule showing a peak at 658.3 MHz. SPAN=660–670 MHz, BW=VBW=30 kHz, SWT=6 s. Tunneling current during spectroscopy 0.3 nA. Bias voltage during spectroscopy 0.3 V. AC field modulation 15 kHz, 10 mG. Lock-in sensitivity 1 mV, time constant 10 ms. (e) ESN-STM peaks were detected at the expected frequency. The horizontal error bar represents the magnetic field range measured over the sample surface. The vertical error bar indicates the frequency range in which the ESN-STM signal was searched for.

Other factors that might account for the discrepancy in the signal intensity with respect to Durkan and Welland's[1] experiments might be the following:

(i) The value of the tunneling current during our ESN-STM experiment is always in the range of 0.3–0.6 nA as opposed to the 1.4 nA used in the Durkan and Welland's one. The lower value of the tunneling current was necessary to avoid damaging the tip and the surface at the location of the tip. In this way we could take several ESN-STM spectra for every scanned image.

(ii) The geometrical capacitance at the tip-sample junction can affect the S/N ratio. Our tips were not chemically etched and therefore may have a larger geometrical capacitance.

(iii) The molecules studied here were deposited on Au(111) and not HOPG surface. Even if it is still not clear how the nature of the surface may affect the signal, internal molecular motion is much probably modified by a different electronic and vibronic environment.[58,59]

VI. CONCLUSIONS

We have detected spin noise at the Larmor frequency in the power spectrum of the tunneling current from two distinct paramagnetic species deposited at the Au(111) surface. These results prove and extend previous experiments by Durkan and Welland[1] but also point out the difficulty of this experiment. We have employed a method of detection designed by Manassen *et al.*[31] and improved it and applied it to the case of physisorbed organic radicals. We give a detailed explanation of our experimental setup to allow interested scientists to have a good starting point to develop their own instrumentation.

The interest in the detection if magnetic resonances through noise has been so far confined to the playground of fundamental physics. However, the current demand for char-

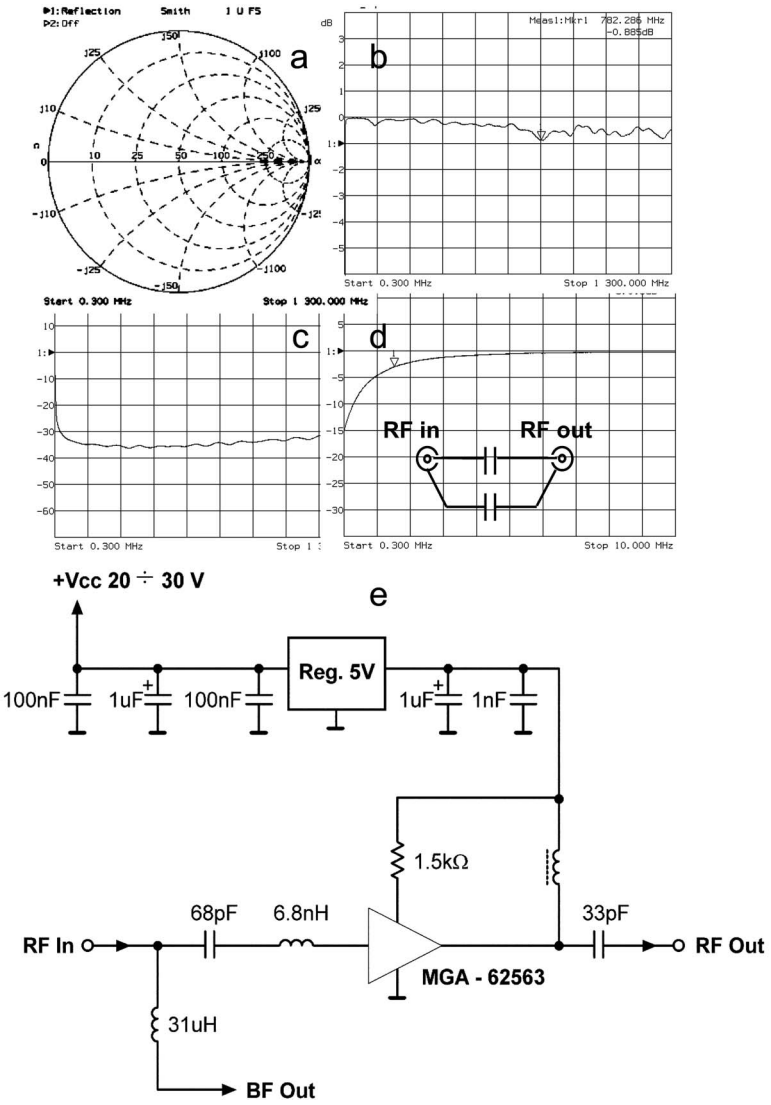

FIG. 9. (a) Impedance measurement of a cable assembly a base plate that simulates the tip-sample geometrical assembly. It can be noted that the impedance is always higher than 50 Ω. (b) Frequency response of the ground decoupler. Insertion loss is less than 1 dB. The circuit diagram is reported in the inset. (c) Frequency response of the dc port of the ac-dc splitter. (d) Frequency response of the ac port of the ac-dc splitter. (e) Circuit scheme for the rf part of the amplifier.

acterization tools at the single molecular level and protocols for spin read out in quantum computing giving impulse to further develop the method for possible future applications. Single spin detection at room temperature, however, poses strong experimental challenges. Our results suggest that future work will have to focus on a rf detection apparatus capable to measure fluctuations on the time scale in which they are generated in a single molecule (detection of transient signals). In other words it will be required to detect frequency fluctuations and to extract signal from the noise in a large detection bandwidth. This is a truly outstanding experimental challenge. Results might also be improved by an appropriate choice of molecular systems, e.g., paramagnetic species with a long T_1 and reduced hyperfine interactions. Also a thorough ultra high vacuum STM study of the candidate molecular specie will be necessary to select molecules that have low diffusion rates on the surface and undergo as small as possible intramolecular rearrangement during the ESN-STM spectral acquisition time.

A further issue is the understanding of the coupling mechanism between the transversal components of the spin vector and the detection apparatus. So far theories have focused on describing how tunneling electrons might couple to the noise while the possibility of near field effects[2,13,26–29] has been ruled out. However, if the coupling between the spin noise detection system and the STM tip were due to a near field effect or a type of electrodynamics pickup[60] it would be possible to design experiments where the tunneling current does not perturb the molecular adsorbates inherently improving the probability to detect the signal.

ACKNOWLEDGMENTS

L. Lenci and C. Ascoli, from the IPCF, Pisa, Italy are acknowledged for providing the magnet and for fruitful discussions. F. Fradin, from ANL, US, is acknowledged for a revision of the manuscript. R. Sergo and A. Grunden, from Elettra, Trieste, Italy, are acknowledged for their technical support. Financial support from the Italian MIUR, FIRB, and FISR projects, Ente Cassa di Risparmio di Firenze EC HPRI-CT-2000-40022 SENTINEL, and MRTN CT-2003 504880 "QuEMolNa" and NMP3-CT-2005-515767 NoE "Magmanet" is also acknowledged. Partial support from the US-Israel Binational Foundation is also acknowledged. Paolo Messina was partially supported by the US DOE-BES under Contract No. DE-AC02–06CH11357.

APPENDIX A

The STM head is placed inside a vacuum chamber. The chamber that provides an easy load for samples with adsorbed molecules on their surface. The pressure reaches 10^{-5} torr within 1 h. The STM head is suspended on stainless steel springs.

The microscope body is divided into two blocks. The bottom part allocates an *X*-*Y* coarse translation stage and the piezotube. The *X*-*Y* coarse positioning stage was added to the system to allow to change the position of the tip over a large area. It is particularly useful to relocate the tip after performing ESN-STM spectroscopy that may locally damage the molecular films (tunneling currents are typically from I_t =0.3 to 1.5 nA). The sample is mounted on the bottom of the upper part of the main body. The coarse approach motion is done by an electrical motor coupled with the feedback controlled *Z* movement of the piezotube.

The STM head top body has a hole allowing the permanent magnet (NdFeB) to slide forward and backward with respect to the sample. The measurement of the magnetic field is accomplished through the Hall probe mounted on top of the sample holder. The probe resolution is 0.1 G (~0.28 MHz for a paramagnet with an electronic Landé factor $g=2.00$); the accuracy is 1% of the reading in the range of 0.1–30 000 G. The magnet is translated by a software controlled electrical motor. A precise homebuilt mechanical positioning device drives the Hall probe over the sample.

The damping system was proven to work effectively. The rf cabling connection does not significantly alter the transfer function of the damping stage. The rf low noise, low level broadband preamplifier is placed close to the STM tip. The decoupling circuit and the dc amplifier are both located inside the case with the rf amplifier. The tunneling current is coupled to the dc amplifier through a set of integrated inductances. These components have a twofold action: on one hand they prevent the rf signal to be lost in the dc part of the circuit; on the other hand they reduce the parasitic capacitance towards the ground seen by the amplifier. The former is required as the maximum amount of rf signal must be transferred to the rf amplifier. The latter is due to the fact that parasitic capacitance seen by the dc amplifier increases the noise at the input. As the dc amplifier is set to detect very low currents, the capacitance must be reduced as much as possible.

The *I*/*V* converter was designed to satisfy two requirements: (i) imaging molecules at low tunneling current (typically 1–10 pA) and (ii) performing ESN-STM spectroscopy on molecules anchored on the surface (I_t=0.3–1.5 nA).

The two major difficulties encountered in the design are the limiting extra Johnson noise coming from the rf amplifier and the noise current at the noninverting terminal due to the stray capacitance.[61,62] The measured noise level for this homebuilt part is 0.6 pA rms. The feedback loop controller can stabilize a current as low as 1 pA.

Because of the ac field applied in time modulated ESN-STM experiments, a four pole homebuilt filter (−3 dB point at 10 kHz) was added to the *I*/*V* converter output to avoid STM feedback oscillations.

To verify the ability of the *I*/*V* converter to work with the operating rf recovery system self-assembled monolayers of hexadecanethiol on Au(111) surfaces were prepared by dipping Au (evaporated on muscovite mica) slides into 1 mM solution of thiol in ethanol, as reported in literature.[63,64] Good STM images were achieved in a pressure of 10^{-5} torr at 2 pA with the rf amplifier switched off and at 20 pA with the rf amplifier switched on.

APPENDIX B

The perfect matching of the junction impedance and the rf input of the rf amplifier at any frequency was not possible. To simulate different STM tip lengths, we built several assemblies consisting of a plate and a coaxial cable with external shield piled out at different lengths. We also embedded these assemblies into Teflon pieces to simulate different rf paths for grounding the shield of the coaxial cable. The inner conductor coaxial cable was brought to different distances from the base plate. This prototype assembly is not measured in tunneling conditions; however, this is not relevant here as the overall impedance of the sample STM tip depends on its geometrical characteristics. The impedance measured in different configurations was always much higher than the amplifier input impedance of 50 Ω. Figure 9(a) shows an example impedance measurement of one of these assemblies. As in our STM design the coaxial cable between the STM tip and the rf amplifier is about 10 cm long; the signal arriving to the amplifier is already adapted to a 50 Ω line. For this reason the input circuit to the amplifier was designed at 50 Ω. The amplifier circuit layout is outlined in Fig. 9(d). The core component is the MGA-62563 (a low noise rf amplifier in E-pHEMET GaAs technology of excellent linearity). The 6.8 nH inductor in the input connector of the MGA-62563 provides the impedance matching between the dc-ac splitter and the input of the MGA-62563. The external resistance of 1.5 kΩ blocks the amplifier polarization current to 40 mA. The characteristics of the amplifier inserted into the circuits allow a noise figure lower than 1 dB.

We also report in Fig. 9(b) the frequency response of the ground decoupler inserted between the rf amplifier and the spectrum analyzer. In the inset we show the scheme of the circuit. The actual mechanical implementation comprises four cylinders coaxially arranged to form two capacitors that decouple the inner and outer connectors of the coaxial cable. In this way the rf part of the signal can travel, but the noise below 2 MHz is prevented to enter the circuitry inside the STM. In our setup the ground decoupler was necessary as the connection of the spectrum analyzer to the ESN-STM provoked some noise on the dc tunneling current used for the STM feedback.

APPENDIX C

Figure 10 shows how a typical spectroscopic mode is implemented in our technique. The STM tip is scanned at low tunneling currents typically between 20 and 30 pA. This is necessary as the tunneling current is also the feedback parameter for the imaging. Good images are achieved only when the STM tip does not approach too much close to the

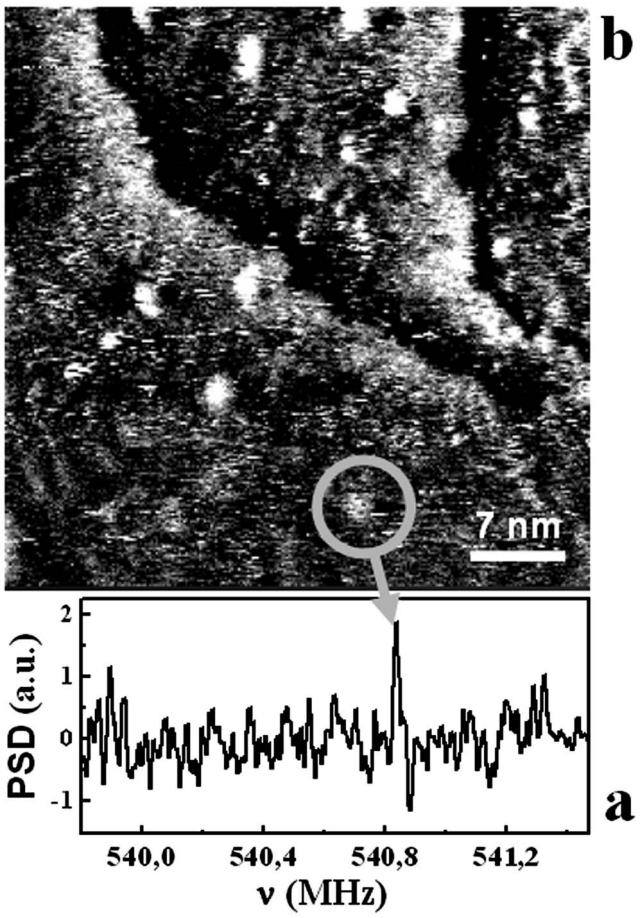

FIG. 10. (a) Typical ESN-STM spectra taken when the STM tip is positioned above the molecule (b) STM image recorded duirng ESN-STM spectra acquisition. The spectrum of (a) corresponds to ESN-STM measurement performed on the white spot evidenced by a circle in (b).

molecule . This is because otherwise its lateral motion during the acquisition of the image would provoke a lateral shift or tumbling of the molecule. During the acquisition of the image the operator chooses a molecule on which to perform the ESN-STM spectroscopy. The software interrupts the lateral motion of the STM tip and then move it to the position corresponding to the selected molecule; the tunneling current is then increased to the optimum value for ESN-STM spectroscopy until the spectrum is acquired. After the acquisition of the spectrum [Fig. 10(a)] correct values for STM imaging are restored, the original position of the tip is recovered and the scan continues. At each point at which the spectroscopy is performed a number and a circle appear on the image [Fig. 10(b)]. On a second monitor we visualize the spectrum acquired Fig. 10(a).

APPENDIX D

In ordinary ESR spectroscopy a microwave field is used to excite transitions between the Zeeman multiplets of a paramagnetic specie. The measurement is possible because there is a net exchange of energy between the system under investigation and the microwave field. The detector measures the difference in energy between the microwave field input into the ESR resonator and the reflected microwave power. The ac modulation of the dc field provokes a time modulation of the Zeeman splitting. This results in a modulation of the ESR signal frequency because the resonant energy moves in time with the ac field. We note that in the ESN-STM detection apparatus described here, the ac modulation of the dc field has a different role.

Indeed as described in a previous paper by one of the authors[13] the frequency of the noise changes periodically with the field modulation, and this, as a result of narrow band detection, leads to the modulation of the output of the spectrum analyzer. Unlike the cw-ESR case, no energy is pumped into or out of the spin system.

[1]C. Durkan and M. E. Welland, Appl. Phys. Lett. **80**, 458 (2002).
[2]T. Sleator, E. L. Hahn, C. Hilbert, and J. Clarke, Phys. Rev. Lett. **55**, 1742 (1985).
[3]S. A. Crooker, D. G. Rickel, A. V. Balatsky, and D. L. Smith, Nature (London) **431**, 49 (2004).
[4]J. Wrochtrup, C. V. Borczyskowski, J. Bernard, M. Orrit, and R. Brown, Phys. Rev. Lett. **71**, 3565 (1993).
[5]D. Gatteschi and R. Sessoli, Angew. Chem., Int. Ed. **42**, 268 (2003).
[6]D. Gatteschi, R. Sessoli, and J. Villain, *Molecular Nanomagnets* (Oxford University Press, Oxford, 2006).
[7]A. M. Ako, I. J. Hewitt, V. Mereacre, R. Clérac, W. Wernsdorfer, C. E. Anson, and A. K. Powell, Angew. Chem., Int. Ed. **45**, 4926 (2006).
[8]Y. Manassen, R. J. Hamers, J. E. Demuth, and A. J. Castellano, Phys. Rev. Lett. **62**, 2531 (1989).
[9]C. Durkan, Contemp. Phys. **45**, 1 (2004).
[10]N. S. Dalal, D. E. Kennedy, and C. A. McDowell, J. Chem. Phys. **59**, 3403 (1973); R. Blehl, K. Moeblus, S. E. O'Connor, R. I. Walter, and H. Zimmermann, J. Phys. Chem. **83**, 3449 (1979); T. Yoshoaka, H. O. Nishiguchi, and Y. Deguchi, Bull. Chem. Soc. Jpn. **47**, 430 (1973).
[11]N. S. Dalal, D. E. Kennedy, and C. A. McDowell, J. Chem. Phys. **61**, 1689 (1974); K. Uchino, J. Yamauchi, H. O. Nishiguchi, and Y. Deguchi, Bull. Chem. Soc. Jpn. **47**, 285 (1974).
[12]A. V. Balatsky, Y. Manassen, and R. Salem, Philos. Mag. B **82**, 1291 (2002); Phys. Rev. B **66**, 161313 (2002).
[13]Y. Manassen, J. Magn. Reson. **126**, 133 (1997).
[14]T. Sleator, E. L. Hahn, C. Hilbert, and J. Clarke, Phys. Rev. B **36**, 1969 (1987).
[15]Y. Manassen and A. V. Balatsky, Isr. J. Chem. **44**, 401 (2004); e-print http://lanl.arxiv.org/abs/cond-mat/0402460.
[16]D. Mozyrsky, L. Fedichkin, S. A. Gurvitz, and G. P. Berman, Phys. Rev. B **66**, 161313 (2002).
[17]J. X. Zhu and A. V. Balatsky, Phys. Rev. Lett. **89**, 286802 (2002).
[18]L. N. Bulaevskii and G. Ortiz, Phys. Rev. Lett. **90**, 040401 (2003).
[19]R. Ruskov and A. N. Korotkov, Phys. Rev. B **67**, 075303 (2003).
[20]J. X. Zhu and A. V. Balatsky, Phys. Rev. B **67**, 174505 (2003).
[21]L. S. Levitov and E. I. Rashba, Phys. Rev. B **67**, 115324 (2003).
[22]L. N. Bulaevski, H. Hrska, and G. Ortiz, Phys. Rev. B **68**, 125415 (2003).
[23]Y. M. Galperin, V. I. Kozub, and V. M. Vinokur, Phys. Rev. B **70**, 033405 (2004).
[24]M. B. Hastings, Phys. Rev. B **70**, 161301(R) (2004).
[25]Z. Nussinov, M. F. Crommie, and A. V. Balatsky, Phys. Rev. B **68**, 085402 (2003).
[26]D. I. Hoult and N. S. Ginsberg, J. Magn. Reson. **148**, 182 (2001).
[27]H. J. Mamin, R. Budakian, B. W. Chui, and D. Rugar, Phys. Rev. Lett. **91**, 207604 (2003).
[28]D. Rugar, R. Budakian, H. J. Mamin, and B. W. Chui, Nature (London) **430**, 329 (2004).
[29]R. Budakian, H. J. Mamin, B. W. Chui, and D. Rugar, Science **307**, 408 (2005).
[30]Y. Manassen, I. Mukhopadhyay, and N. Ramesh Rao, Phys. Rev. B **61**, 16223 (2000).
[31]Y. Manassen, E. Ter Ovanesyan, D. Shachal, and S. Richter, Phys. Rev. B **48**, 4887 (1993).
[32]Agilent Technologies Report No. 5952-0292 (unpublished) (http://cp.literature.agilent.com/litweb/pdf/5952-0292.pdf).
[33]The measured magnetic field was determined by using the vector sum: $\|\mathbf{B}(x,y,z)\| = \sqrt{B_x^2 + B_y^2 + B_z^2}$. The error is calculated accordingly.
[34]R. Basu, J. D. Tovar, and M. C. Hersam, J. Vac. Sci. Technol. B **23**, 1785

(2005).
[35]J. V. Barth, Surf. Sci. Rep. **40**, 75 (2000).
[36]P. Messina, A. Dmitriev, N. Lin, H. Spillmann, M. Abel, J. V. Barth, and K. Kern, J. Am. Chem. Soc. **124**, 14000 (2002).
[37]C. Kikuchi and V. N. Cohen, Phys. Rev. **93**, 394 (1954).
[38]Yu. A. Koksharov, I. V. Bykov, A. P. Malakho, S. N. Polyakov, G. B. Khomutov, and J. Bohr, Mater. Sci. Eng., C **22**, 201 (2002).
[39]A. Abragam and B. Bleaney, *Electron Paramagnetic Resonance of Transition Ions* (Dover, New York, 1986), p. 527.
[40]J. P. Goldsborough, M. Mandel, and G. E. Pake, Phys. Rev. Lett. **4**, 13 (1960).
[41]J. P. Lloyd and G. E. Pake, Phys. Rev. **92**, 1576 (1953).
[42]J. A. Weil, J. R. Bolton, and J. E. Wertz, *Electron Paramagnetic Resonance, Elementary Theory and Practical Applications* (Wiley, New York, 1994), p. 462.
[43]W. C. Van Etten, Introduction to Random Signals and Noise (Wiley, Chichester, England, 2005), pp. 101 and 115.
[44]J. P. Wolfe, Phys. Rev. Lett. **31**, 907 (1973).
[45]T. Maly, F. MacMillan, K. Zwicker, N. K. Poor, U. Brandt, and T. F. Prisner, Biochemistry **43**, 3969 (2004).
[46]S. S. Eaton and G. R. Eaton, J. Magn. Reson., Ser. A **102**, 354 (1993).
[47]G. J. Kruger, Adv. Mol. Relax. Processes **3**, 235 (1972).
[48]G. J. Kruger, Z. Naturforsch. A **24A**, 560 (1969).
[49]R. Brandle, G. J. Kruger, and W. Muller, Z. Naturforsch. A **24A**, 111 (1970).
[50]R. Rosest and N. J. Poulis, Physica **25**, 1253 (1959).
[51]I. Miyagawa, K. Sogabe, and S. A. Hossain, Chem. Phys. Lett. **182**, 668 (1991).
[52]D. Pierreux and A. Stesmans, Phys. Rev. B **66**, 165320 (2002).
[53]T. Umeda, M. Nishizawa, T. Yasuda, J. Isoya, S. Yamasaki, and K. Tanaka, Phys. Rev. Lett. **86**, 1054 (2001).
[54]W. Futako, N. Mizuochi, and S. Yamasaki, Phys. Rev. Lett. **92**, 105505 (2004).
[55]W. B. Mims, *The Linear Electric Field Effect in Paramagnetic Resonance* (Clarendon, Oxford, 1976).
[56]P. P. Yodzis and W. S. Koski, J. Chem. Phys. **38**, 2313 (1963).
[57]B. Cage and S. Russek, Rev. Sci. Instrum. **75**, 4401 (2004).
[58]G. Alzetta, E. Arimondo, and C. Ascoli, Nuovo Cimento B **54**, 163 (1968).
[59]DPPH was not used as spin probe for other single spin detection experiments.
[60]While the manuscript was in preparation we became aware that another group has achieved similar results on a different spin probe (TEMPO-L) deposited on Au(111). W. Olejniczak, P. Krukowski, P. Kobierski, S. Pawlowski, and K. Gwozdzinski, Fourth International Conference on Tribochemistry, Krakow, 3–5 October 2005 (unpublished).
[61]M. Carlà, L. Lanzi, E. Pellecchi, and G. Aloisi, Rev. Sci. Instrum. **75**, 497 (2004).
[62]L. Libioulle, A. Radenovic, E. Bystrenova, and G. Dietler, Rev. Sci. Instrum. **74**, 1016 (2003).
[63]F. Schreiber, Prog. Surf. Sci. **65**, 151 (2000).
[64]R. K. Smith, P. A. Lewis, and P. S. Weiss, Prog. Surf. Sci. **75**, 1 (2004).